Journal of Computational Electronics (2026) 25:32
https://doi.org/10.1007/s10825-025-02480-6

Broadband high-temperature metamaterial absorber and thermal emitter composed of fractal geometry

Khaled Aliqab[1] · Ammar Armghan[1] · Spyridon Nektatios Daskalakis[2] · Meshari Alsharari[1]

Received: 30 June 2025 / Accepted: 18 December 2025 / Published online: 4 January 2026

Abstract

Fractal structures are natural patterns that repeat themselves. They have several unique features that make them ideal for solar energy absorption and sensing applications. In this study, we present a high-performance, polarization insensitive solar absorber comprises of a nickel (Ni)-made hash-shaped fractal geometry develop over a thin layer of gallium-doped zinc oxide (GZO) features a high absorption rate that covers the visible and near-infrared wavelengths of the spectrum. The results show that broadband aggregative absorptivity of 92% is attained between 380 nm and 3850 nm attributed to remarkable localized surface plasmon resonance (LSPR) induced by the periodic array of Ni nano-resonators and surface plasmon resonance (SPR) at the interface of GZO-SiO_2 layers. Further, the absorptivity remains above 90% from 670 nm to 3850 nm over a bandwidth of 3180 nm. With the utility of high-temperature resilient materials in the developed metamaterial structure, it shows potential for the thermal applications; as the results indicate the maximum heat radiation efficiency is 92.88% at 1600 K. Aside from that, we provide insight into the broadband high solar light capturing characteristics of the proposed device with the support of surface current density and electric field distribution study at the selective wavelengths. Furthermore, the device's parametric study revealed a minor impact on its absorptivity/emissivity characteristics while also suggesting its robustness, which could be useful in device manufacture process. The overall benefits of the proposed device show its potential for high-temperature solar energy harvesting applications and solar thermophotovoltaic (STPV) cells.

Keywords Fractal geometry · Metamaterial · Ultrathin · Solar energy · Thermal radiation · Broadband · Photonics device

1 Introduction

Nanostructures based on metamaterials, sized at a fraction of the operating wavelength, can effectively capture solar energy and emit thermal radiation [1–4]. Their exceptional ability for light wave absorption suggests potential utility in various domains, including solar cells for energy harvesting, sensors for the biomedical and chemical industries, and thermal emitters for STPV systems [1–11]. Moreover, by tailoring the nanostructures, they can be made useful to operate in different frequencies windows including ultraviolet (UV), visible, and infrared regimes [12–19].

✉ Ammar Armghan
aarmghan@ju.edu.sa

[1] Department of Electrical Engineering, College of Engineering, Jouf University, 72388 Sakaka, Saudi Arabia

[2] School of Engineering and Physical Sciences, Institute of Sensors, Heriot Watt University, Edinburgh, UK

Metamaterials-based optical absorbers are often classified into two types based on their operation: wideband and narrow/selective band, depending on the intended application [12–23]. For example, wideband solar absorbers with strong absorption properties in the visible and infrared regions are well-suited for energy harvesting applications [22, 23], TiN-based solar absorber and thermal emitter have been discussed [24–26]. Also, fractal structures are utilized to enhance the absorptivity [14, 16, 17], these fractals resonators operate on LSPR across various wavelengths. All of the aforementioned mechanisms come from the interaction of electromagnetic waves with the nanoscale structure of the solar energy absorbing device to achieve high absorptivity/emissivity properties [22–26].

Specific to the wideband solar absorbers, numerous studies indicate their operation in the visible and near-infrared spectra [12–19, 27, 28]. For instance, authors in ref. [12] report that a conical-shaped wideband absorber made of SiO_2 and Al operates in the visible region (400–1000 nm) with a solar absorption efficiency of 90%.

Metal–dielectric-based several studies demonstrated that metamaterial solar absorbers, made of different materials, achieve with a solar absorption rate of 90% and above and exhibit angular stability up to 40° [28, 31–34]. Recent studies have focused on metamaterial-based thermal emitters for passive radiative cooling applications. It has been reported that a machine learning-assisted dielectric metasurface-based passive radiative cooler can effectively reduce temperature by up to 15.4 °C [35]. Wang et al. [36], investigated a daytime passive radiative cooler which show high solar spectrum reflection up to 92% and a temperature reduction of 9.5 °C.

Motivated by these studies, we present a study of polarization insensitive ultrathin broadband fractal geometry-based solar absorber made of high-temperature resilient materials that operates in the visible, near-infrared and mid-infrared spectral ranges. The constituents of the developed solar absorber are nickel (Ni), tungsten (W), silicon dioxide (SiO_2) and gallium-doped zinc oxide (GZO) have high melting points (of > 1400 °C) [37–41] and thermally stability which make it suitable for high-temperature thermal applications and solar energy harvesting. As the result of strong localized surface plasmon resonance (LSRP) due to the fractal structure of the top metasurface layer and surface plasmon resonance (SPR) at the interface of GZO-SiO_2 layers, results in solar absorption efficiency of 92% within the 380 nm–3850 nm wavelength spectrum. The structure's symmetry of the metasurface ensures stability of polarization of the incident light and absorptivity remains stable up to 50°. The proposed solar absorber design possesses the potential for thermal emitter applications at high temperature.

2 Device design and simulation

Figure 1 presents the solar absorber 3D panel made of periodically arranged unit cell of fractal hash-shaped top layer geometry, along with 2D view of unit cell with necessary geometric information and step wise details of fabrication process. The unit cell comprises of three layers; where top layer is made of nickel (Ni) featuring a hash-shaped etched fractal geometry, followed by gallium-doped zinc oxide (GZO) on substrate layer of SiO_2, which has a dielectric constant of 2.25 [22]. A thick tungsten (W)-made

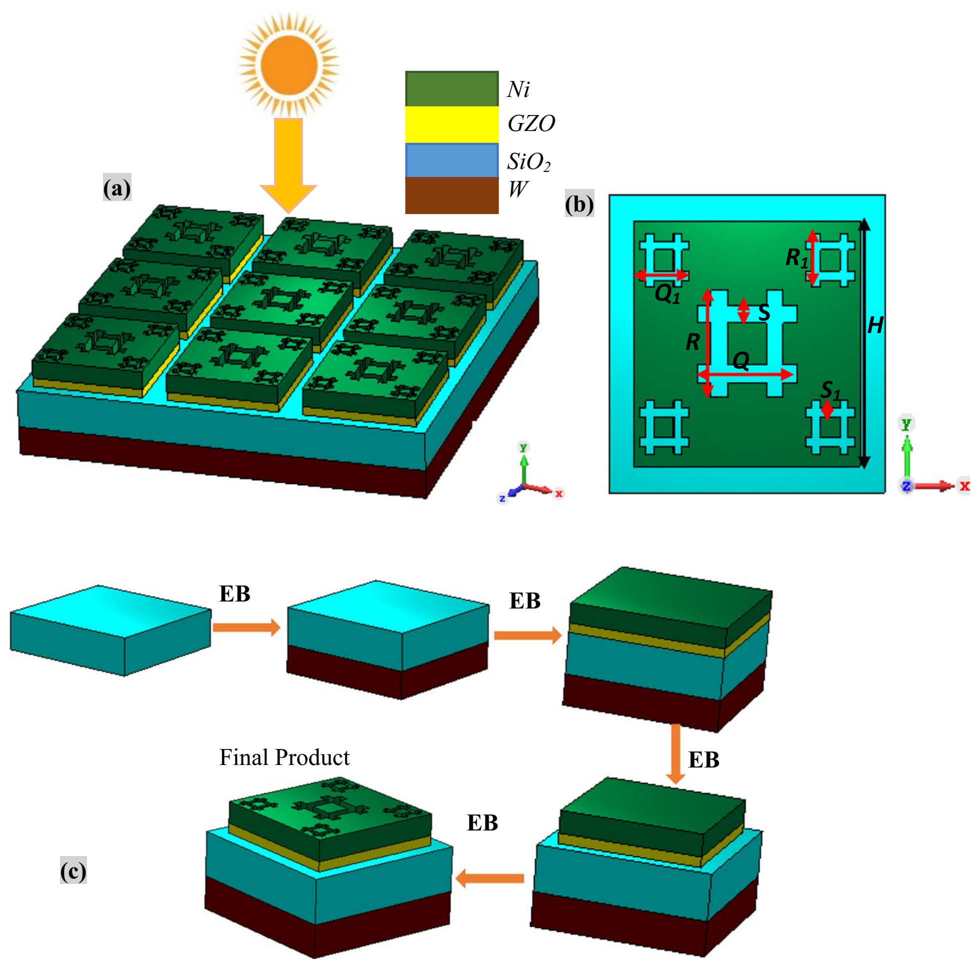

Fig. 1 **a** 3D view of fractal-shaped solar absorber/emitter panel, **b** 2D view of the unit cell representing top layer geometric information, and **c** fabrication procedure of the developed unit cell design

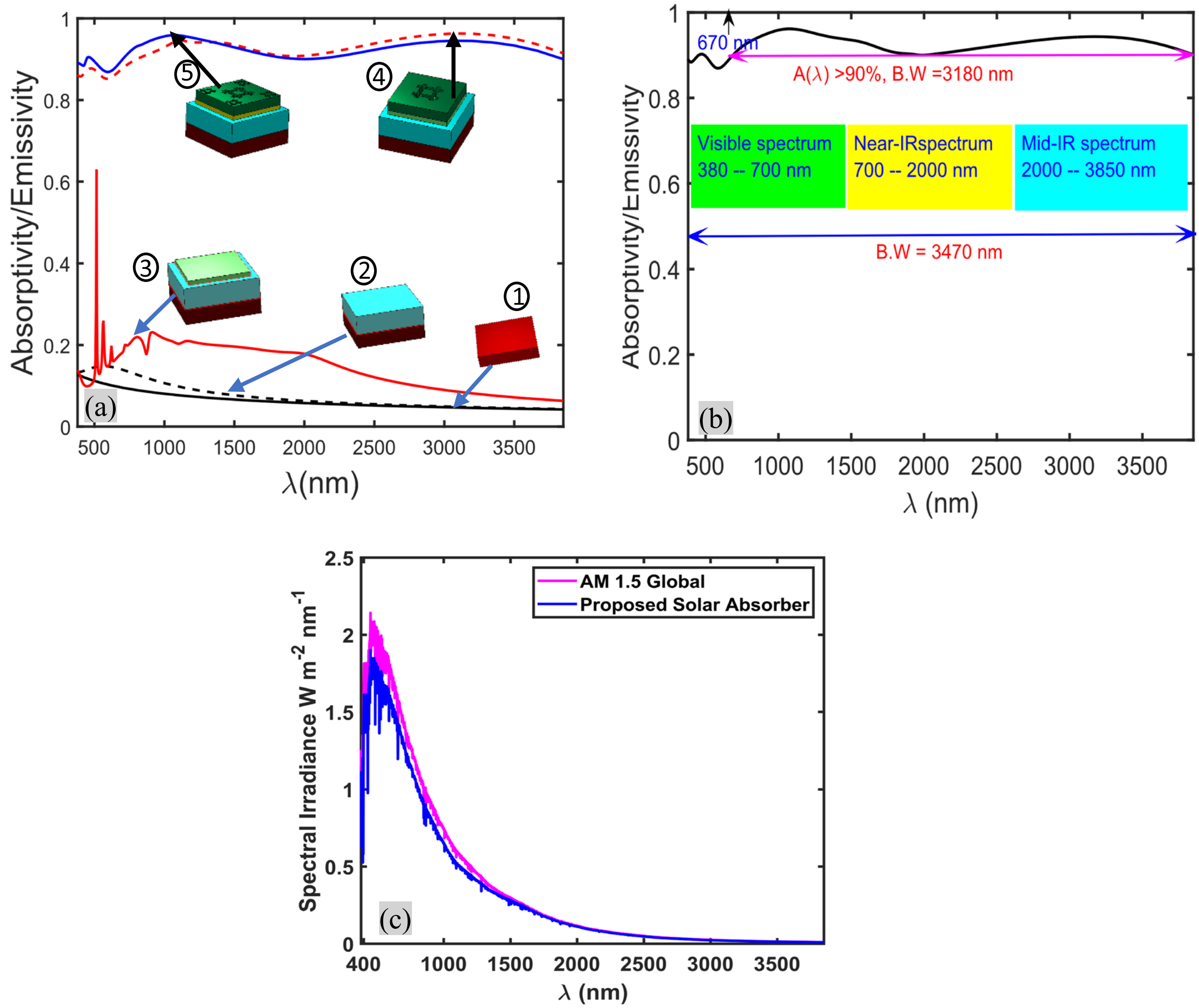

Fig. 2 Absorptivity of solar absorber; **a** absorption detail of layered structure, **b** detailed information of the optimum design-based solar absorber and **c** comparison with AM 1.5 solar spectra

bottom layer is utilized for the reflection of light waves. As described above, the utilized materials in the design of the solar absorber features with high-temperature resilient and thermally stable. Here, we provide the geometrical information of the fractal-shaped solar absorber is given as follows: The panel of the proposed absorber/emitter (presented in Fig. 1a) which is comprised of periodic unit cells period $P = 500$ nm. The thicknesses of four-layers structure from top to bottom are defined as $t_3 = 65$ nm for Ni, $t_2 = 30$ nm for the GZO, $t_1 = 135$ nm for SiO_2, and $t = 100$ nm for W. The dimensions of the top fractal layer (in Fig. 1b), are specified as $H_x = H_y = H = 410$ nm, $Q = R = 360$ nm, $S = 30$ nm, and $Q_1 = R_1 = 180$ nm, $S_1 = 15$ nm, respectively.

The top two layers effectively absorb the light waves owing to the optimized geometric configuration of the Ni-based fractal geometry, which induces strong localized surface plasmon resonance (LSPR) and at the interface of thin layer of GZO and substrate, surface plasmon resonance (SPR) further enhance the light energy absorption. The substrate layer retains the absorbed energy within the structure, while the W-based layer at the bottom preventing light wave transmission. The proposed solar absorber, with a Ni-made fractal-shaped geometric design along with optimized dimensions of the thin layer of GZO, exhibits significant solar absorption, facilitating the capture of light waves over the broad spectral range.

The fabrication process for the solar absorber\thermal emitter, made of four distinct layers, is explained and depicts in Fig. 1c. The proposed design is realized through the utilization of micro/nano-manufacturing techniques. The

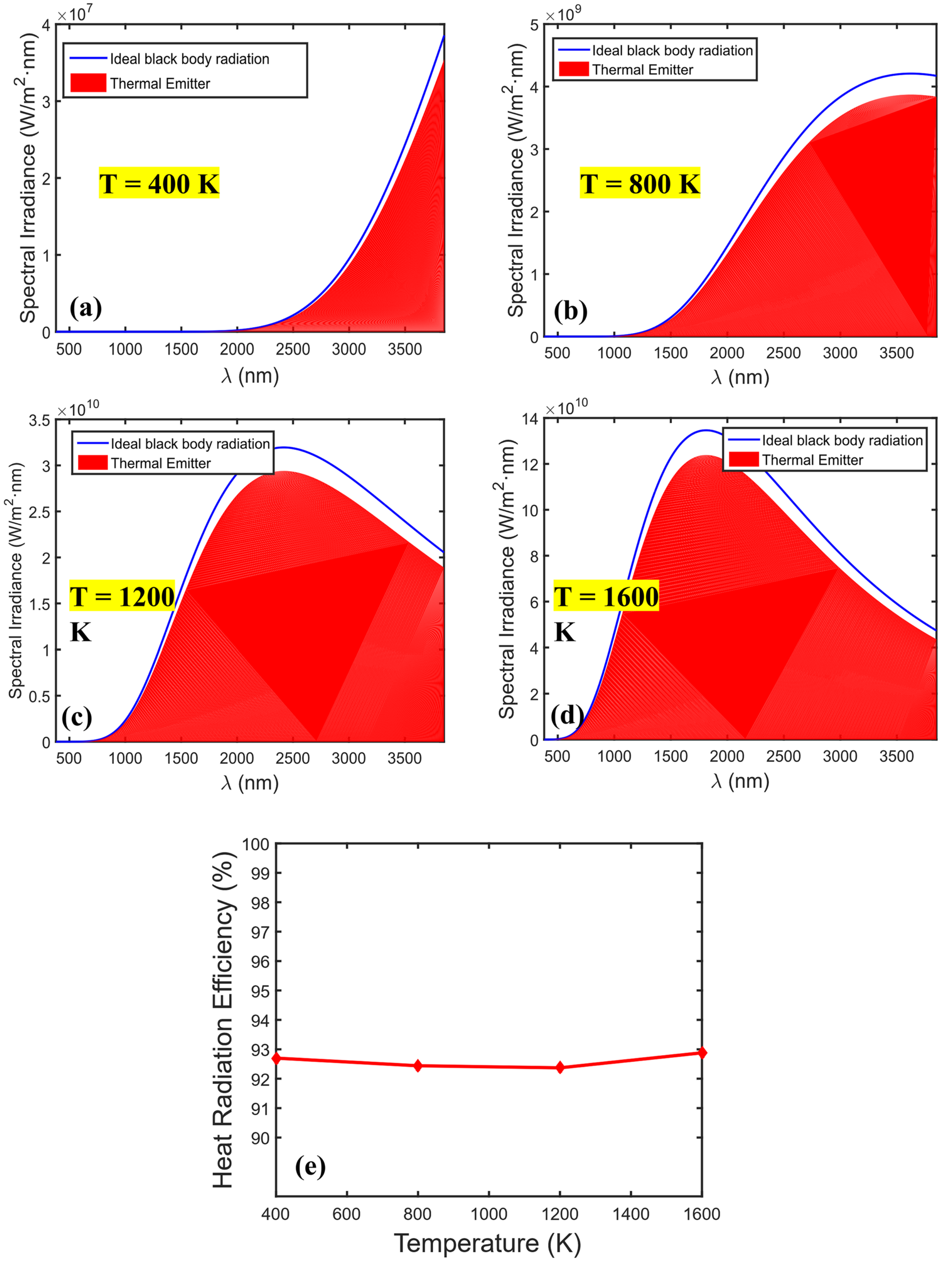
×10^7
Ideal black body radiation
Thermal Emitter
T = 400 K
(a)
Spectral Irradiance (W/m^2·nm)
λ (nm)
×10^9
Ideal black body radiation
Thermal Emitter
T = 800 K
(b)
Spectral Irradiance (W/m^2·nm)
λ (nm)
×10^10
Ideal black body radiation
Thermal Emitter
T = 1200 K
(c)
Spectral Irradiance (W/m^2·nm)
λ (nm)
×10^10
Ideal black body radiation
Thermal Emitter
T = 1600 K
(d)
Spectral Irradiance (W/m^2·nm)
λ (nm)
Heat Radiation Efficiency (%)
(e)
Temperature (K)

◂**Fig. 3** **a**–**d** represent thermal emitter radiation spectra for different conditions of operating temperature 400 K, 800 K, 1200 K, and 1600 K, respectively, and **e** thermal radiation efficiency versus temperature

construction of the suggested absorber/thermal emitter consists of multiple stages as follows: The initial step involves electron beam deposition—a thin layer of tungsten (W) is applied to the bottom-side of the SiO_2 substrate. In the second step, a thin layer of gallium-doped zinc oxide (GZO) and a thin layer of nickel (Ni) are deposited on the upper surface of the SiO_2 substrate, as illustrated in the figure. The subsequent, third stage involves electron beam lithography (EBL) and the lift-off process. The concluding method, EBL, lift-off procedure, and the photoresist are exposed to create a grating array structure [29, 30].

We evaluate device's absorption [23] as $A(\lambda) = 1 - [R(\lambda) + T(\lambda)]$ using specified parameters. $R(\lambda)$ and $T(\lambda)$ are the reflectance and transmittance at wavelength λ, respectively, and can be defined in terms of S-parameters as $R(\lambda) = |S_{11}|^2$ and $T(\lambda) = |S_{21}|^2$. Here, S_{11} and S_{21} are reflection and transmission coefficients, respectively. The term $T(\lambda)$ becomes zero as a result of the thick W bottom layer. According to Thermodynamics law, solar energy absorbed by the medium is equivalent to the emissivity $\varepsilon(\lambda)$; therefore, it can be formulated as $\varepsilon(\lambda) = A(\lambda)$. To attain S_{11}, boundary conditions on the unit cell along the *x*- and *y*-axis are employed in the CST software, with a light wave in the spectral range of 380 nm–3850 nm incident on the upper metasurface layer of the absorber structure and propagating along the *z*-axis.

The spectral AM 1.5 can be calculated as [32]

$$\eta_{abs} = \frac{\int_{\lambda \min}^{\lambda \max} [A(\lambda) \times I_{AM1.5}(\lambda) d\lambda}{\int_{\lambda \min}^{\lambda \max} I_{AM1.5}(\lambda) d\lambda} \quad (1)$$

where $\lambda_{min} = 380$ nm and $\lambda_{max} = 3850$ nm, and $I_{AM1.5}(\lambda)$ defines the solar irradiation spectrum as a function of wavelength.

For studying thermal emitter characteristics of our developed metamaterial-based nanostructure made of high-temperature and oxidation resilient materials, we evaluate the device performance with heat radiation efficiency under high-temperature conditions up to 1600 K. The heat radiation efficiency is defined as [32]:

$$\eta_{E} = \frac{\int_{\lambda \min}^{\lambda \max} [\varepsilon(\lambda) \times I_{B}(\lambda, T) d\lambda}{\int_{\lambda \min}^{\lambda \max} I_{B}(\lambda, T) d\lambda} \quad (2)$$

In above Eq. (2), $\varepsilon(\lambda)$ is the emissivity of the thermal emitter, $I_B(\lambda, T)$ denotes the intensity of ideal black body radiation, depending upon wavelength and temperature.

3 Results and discussion

Figure 2a illustrates the absorptivity/emissivity characteristics of the absorber, considering it layered structure. Each layer's impact on absorptivity is analyzed. Absorptivity increases with the addition of layers. The incorporation of Ni hash-shaped layer has improved absorption within the visible solar spectrum. Figure 2b illustrates the absorptivity/emissivity spectra of the proposed solar absorber. The figure shows the absorptivity curve spanning over the wide spectral window ranging from 380 nm to 3850 nm. The broad absorptivity/emissivity arises from the pervasive LSPR and SPR causes by the top two layers geometry. The absorptivity/emissivity of the developed device cover broadband spectrum including visible, near-infrared and mid-infrared regimes. The absorptivity/emissivity plot shows the total absorptivity/emissivity of 92% within the 380 nm–3850 nm spectrum. The absorptivity/emissivity remains above 90% from 670 nm to 3850 nm. Due to the broadband high absorptivity/emissivity characteristics and utility of high-temperature resilient materials in its development, the device is potentially useful for the high-temperature solar energy harvesting, thermal emitter applications, and infrared imaging and sensing. Figure 2b demonstrates the comparison of the developed solar absorber light energy capturing ability with comparison to the standard solar AM1.5 spectral radiation model curve. It is clearly depicted that the developed device is showing spectral matching with the standard solar AM model and therefore, can be useful for the highly efficient solar cells-based applications. Dendrite-based, square-shaped and Sierpinski fractals [14, 16, 17] have been reported for solar absorber applications; however, a comparison of the proposed absorber with existing fractal absorbers has demonstrated superior results.

Using (2), Fig. 3 illustrates the thermal emission spectra of the developed metamaterial structure for different operating temperature conditions. The red shaded area demonstrates the thermal emitter radiations curve of our developed nanostructure, and the blue line curve demonstrates the spectral irradiance of the ideal blackbody radiations over the operating spectrum. Considering Fig. 3a, it is noticed that the spectral irradiance of blackbody and thermal emitter has good agreement. Figure 3b and c demonstrates the spectral irradiance for operating temperature 800 K and 1200 K, respectively. It is observed that spectral radiations increased with the increase the temperature. Figure 3d depicts the emission spectra for 1600 K, it is observed that the radiation intensity is improved in vis. and NIR spectra for higher operating temperature. These features of thermal emitter make it potentially useful for the high-temperature thermal applications. Figure 3e shows the heat radiation efficiency vs operating

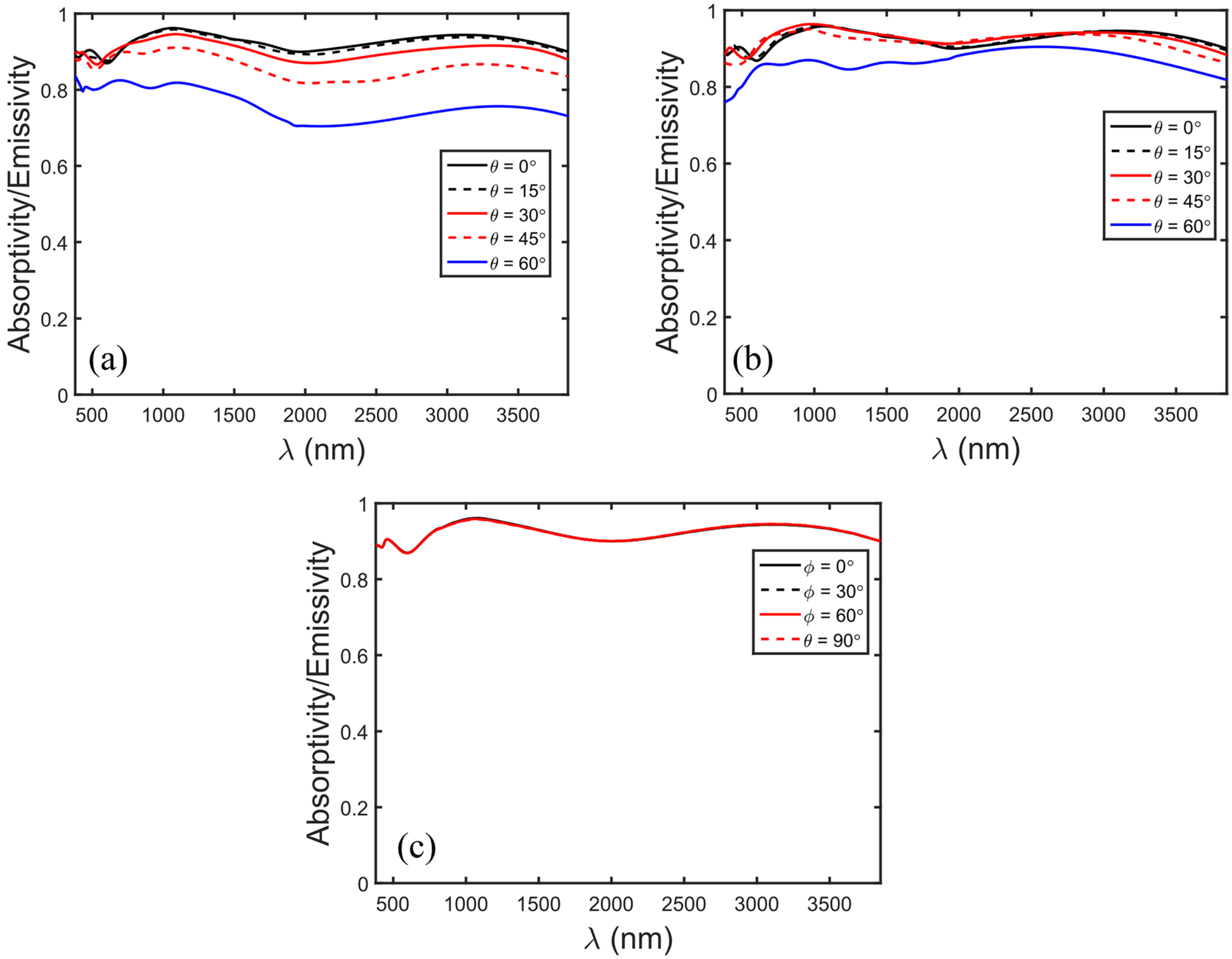

Fig. 4 Absorption spectra for oblique incident **a** for TE mode, **b** for TM modes and **c** polarization angle for TM mode

temperature ranging from 400 K to 1600 K. This curve shows the thermally stable behavior of the developed metamaterial-based structure where heat radiation efficiency shows a minimal variation from 92.37 % to 92.88% over the temperature range of 400 K–1600 K. Therefore, the developed device possesses the potential for its possible use for the high-temperature thermal applications.

For the most of engineering applications, polarization insensitive nature and wide angular stability of the solar absorber/thermal emitter devices are desirable. Therefore, we studied the impact of the polarization and obliquity of incident light on absorptivity/emissivity of the proposed solar absorber. Figure 4a shows the absorptivity/emissivity plot for TE mode at various incidence angles ranging from 0° to 60° for this mode, the angular stability is high (up to 50°) to maintain the high absorption characteristics. Figure 4b presents the absorptivity spectra plot for the TM mode. The absorptivity is noticed to be significantly higher in comparison with the TE mode. The angular stability in this scenario reaches up to 60° to maintain high absorption properties as illustrated in Fig. 4b. The higher angular stability of the proposed absorber makes it suitable for thermal emitter applications. Further, effects of the polarization on absorptivity are considered. Figure 4c illustrates the absorptivity for different polarization angles, indicating no significant variation in absorption attributable to the symmetrical geometry of the top layer of developed structure. In conclusion, LSPR conditions exhibits insensitivity to the polarization of the incoming light waves, rending the absorber advantageous for industrial applications.

The examination of surface current density and electric field distribution aids in understanding the absorption mechanism of light waves within the developed device. Therefore, Fig. 5 demonstrates the flow of surface current on the top and bottom layer of the absorber. Figure 5a and b illustrates the surface current for a wavelength of 700 nm in the top and bottom layers, respectively. The surface current densities, represented by arrow shaped vectors, of top and

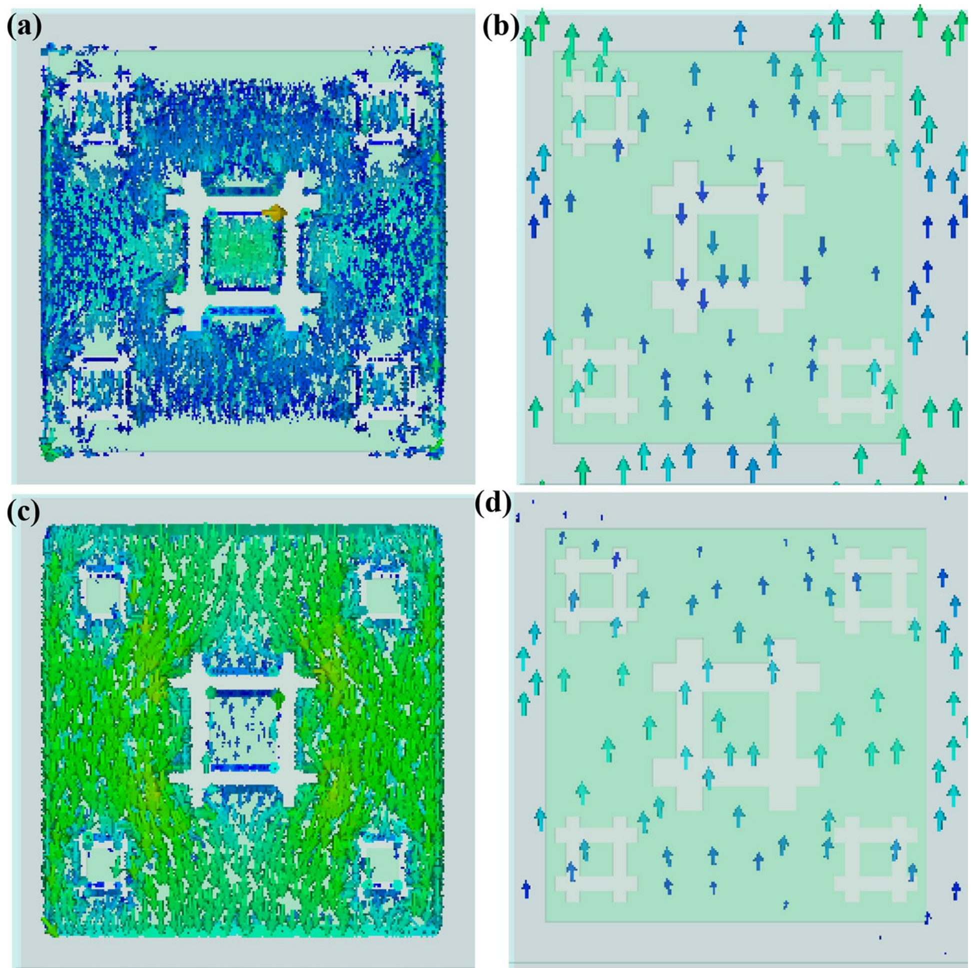

Fig. 5 Surface current densities of the metasurface absorber **a** 700 nm (top layer), **b** 3500 nm (bottom layer), **c** 700 nm (top layer) and **d** 3500 nm (bottom layer)

bottom layers appeared to be parallel to one another, exhibiting the phenomenon of electric resonance. Consequently, LSRP results from the electric resonance. Surface currents for the top and bottom layers at the operating wavelength of 3500 nm are presented in parts (c) and (d) of Fig. 5, exhibiting a trend analogous to that observed in the previous case. Electric resonance is inferred to induce the strong LSPR within the solar absorber structure.

Further, the electric field patterns of the top metasurface is analyzed for high absorptivity wavelengths such as 670 nm, 1100 nm, 2000 nm and 3850 nm, as illustrated in Fig. 6a–d. The figures indicate that the electric field is significantly confined within the metallic resonators of the top metasurface for the lower operating wavelengths 670 nm, 1100 nm (as shown in Fig. 6a and b). Consequently, this results in broadband high absorptivity. For higher wavelength 2000 nm and 3850 nm, the electric field is remains confined on the interface of GZO and Ni as depicted in Fig. 6c and d. The field trapped at the top resonator surface lead to LSPR, and field trapped at the interface of Ni, GZO and SiO_2 attribute to SPR. Henceforth, absorption is due to LSPR and SPR.

Aforesaid results show the absorption results of the optimized structure of proposed absorber. Figures 2, 3 and 4 illustrate the absorptivity/emissivity spectra associated with the optimized parametric values. Here, we discuss the impact of altering the geometric parameters of the device on its absorption characteristics. Figure 7a presents the absorption considering period of the unit cell of fractal metamaterial absorber. The results show that optimized absorptivity/emissivity is attained for $P = 500$ nm. It can be observed that variation in the dimension of the period of the unit cell has a minor effect on overall absorptivity spectra. Therefore, the proposed device has manufacturing tolerance for unit cell period. Figure 7b shows the effect of GZO layer thickness (t_2) on the absorptivity/emissivity. The results indicate that variation in the absorptivity curves is minimal over the entire operating band for all thicknesses values examined, which range from 20 nm to 40 nm. The optimal absorptivity curve is attained with a substrate layer thickness of 30 nm. In a similar manner, Fig. 7c shows the effect on the absorptivity while varying the thickness of the top metasurface layer (t_3) from 55 nm to 75 nm in increments of 5 nm. The results show that changes in the thickness of the top metasurface

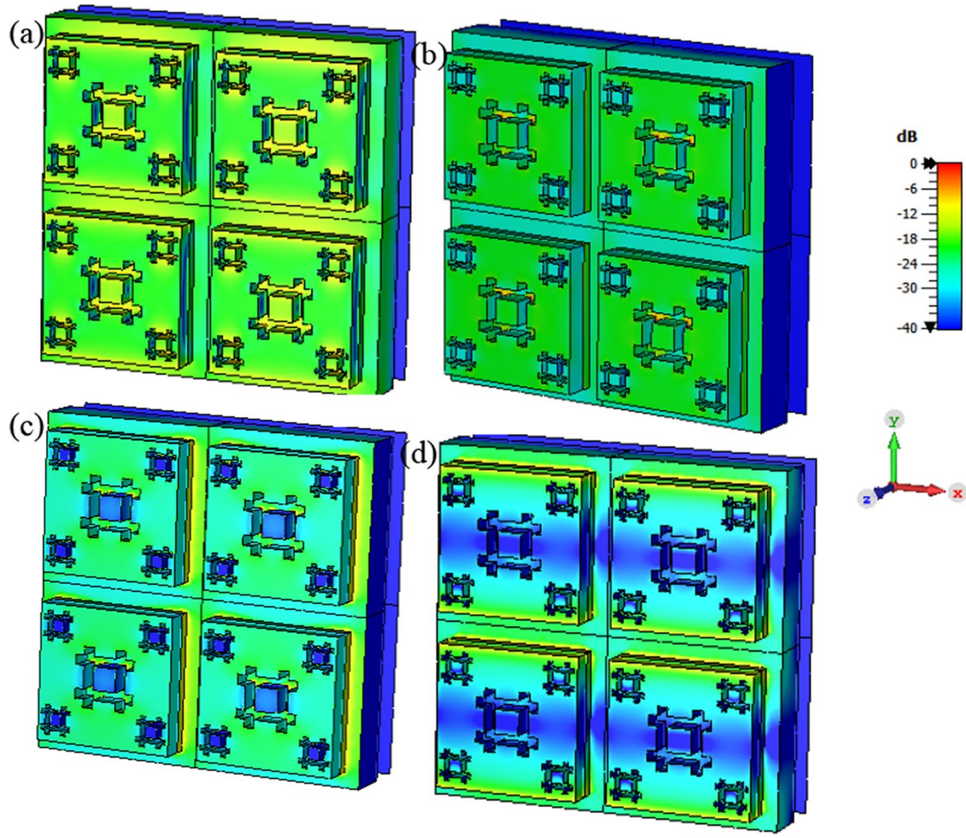

Fig. 6 Electric field distribution patterns at the wavelengths of **a** 670 nm, **b** 1100 nm, **c** 2000 nm and **d** 3850 nm

layer have a negligible effect on the absorptivity of the proposed absorber. The optimal results for the absorption are attained at 65 nm. The analysis reveals that the developed solar absorber exhibits considerable resilience to variations in geometric parameters, thereby, maintaining stable performance. The aforesaid discussion indicates that the proposed device exhibits a high level of fault tolerance.

Table 1 presents a comparative overview of several recent relevant published studies concerning metamaterial solar absorbers/emitter operate in the visible and near-infrared regimes with our work. The developed structure demonstrates ultrathin dimensions, a relatively simple design, a high absorptivity/emissivity rate, excellent thermal radiation efficiency under high temperature conditions, attributed to the incorporation of high-temperature resilient materials. Additionally, it exhibits wideband operational capabilities in the visible and near-infrared regions when compared to the works documented in the table. The developed metamaterial-based structure design indicates potential for high-temperature solar energy harvesting and thermal applications.

4 Conclusion

The aforementioned discussion reveals that the developed ultrathin broadband fractal-shaped metamaterial absorber and thermal emitter operate within the visible and near-infrared regimes. The findings show that the designed nanostructure, made from high-temperature resilient materials, attains a total absorptivity/emissivity of 92% across 380–3850 nm spectral range and demonstrates exceptional thermal radiation efficiency exceeding 92.88% at 1600 K. The strong light waves absorption across the broadband spectrum attributes to LSPR induced by the top metasurface metal-made fractal geometry. Furthermore, the examination of surface current and surface electric field at high-absorption wavelengths has provided insight details about the light wave absorption. The device's design symmetry exhibits polarization robustness and maintains angular stability up to 50°. Moreover, results depict that developed device would be useful for solar energy harvesting applications and has consistent efficiency under high-temperature operating conditions.

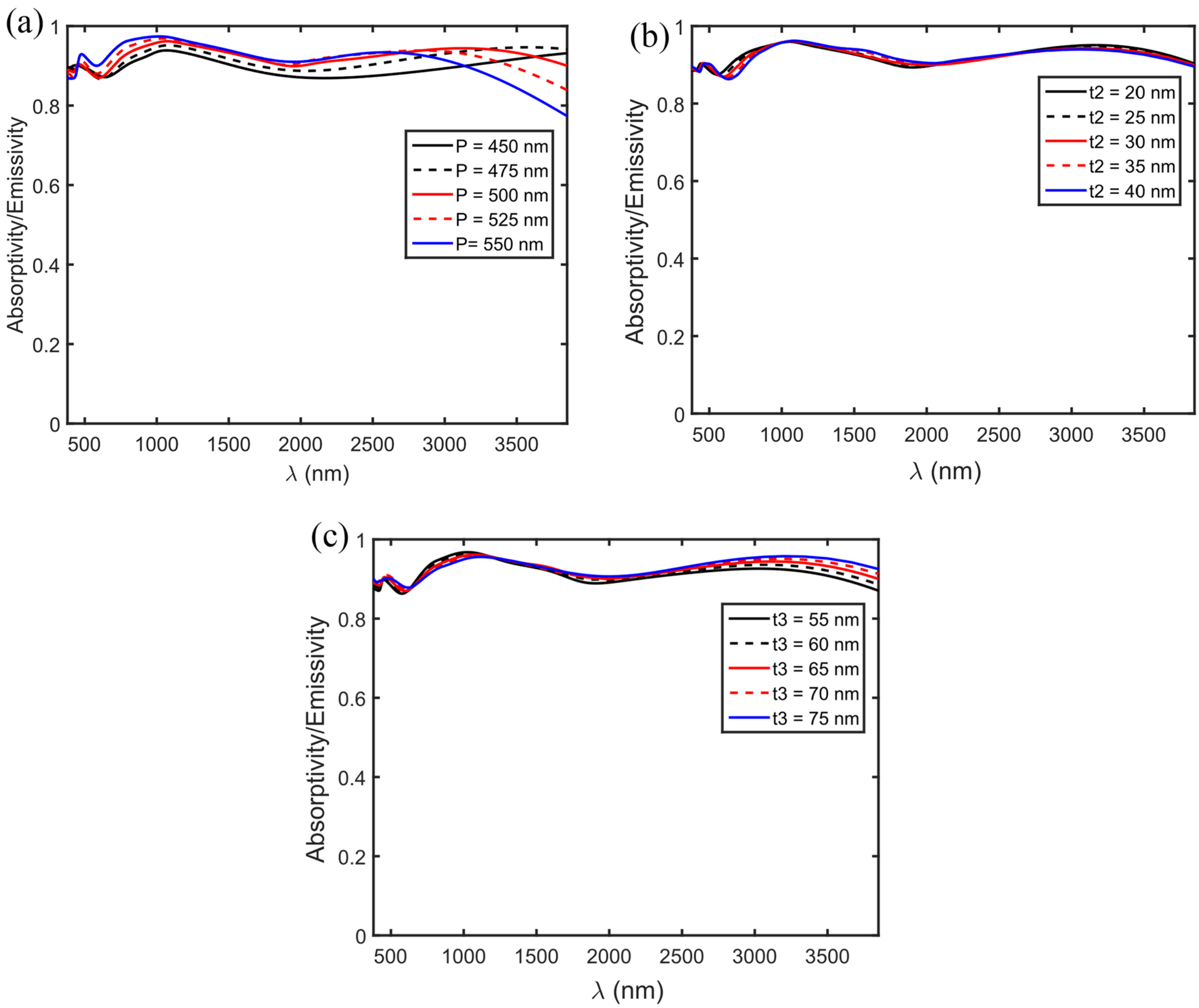

Fig. 7 Impact of the variation in structural parameters of the absorber on the absorption spectra; **a** period of the unit, *P* **b** thickness of GZO, t_2 and **c** thickness of top layer, t_3

Table 1 Comparison of relevant existing studies with the proposed work

References	Operating region (nm)	Unit cell material composition	Avg. Thermal Emissivity	Operating band-width > 90%(nm)	Thermal Radiation Efficiency	Polarization robustness/angular stability
This work	380–3850	Ni, GZO-W	> 90	3180	92.8@ 1600 K	Yes/up to 50°
[14]	300–2500	TiN–SiO_2	> 90	2200	–	Yes/up to 50°
[31]	300–2500	MXene-SiO_2	> 90	2200	–	–
[32]	300–3000	SiO_2–Ti	> 90	2382	94% @ 1000 K	Yes/up to 40°
[33]	280–3000	Ti–SiO_2	> 90	1645	94.4%@ 1000 K	Yes/up to 50°
[34]	300–2200	HfO_2-W	> 90	1900	87% @1600 K	Yes/up to 60°
[41]	260–3000	Ti–SiO_2	> 90	2720	94.4% @1600 K	–
[42]	280- 2500	Mo	> 90	2220	41.8@ 1723 K	–
[43]	200–300	MXene	> 80	2800	–	Yes/up to 60°

Acknowledgements This work was funded by the Deanship of Graduate Studies and Scientific Research at Jouf University under grant No. (DGSSR-2025-02-01463).

Authors contributions K. Aliqab, A. Armghan, S. N. Daskalakis and M. Alsharari contributed to conceptualization, methodology, writing—original draft, and project administration. K. Aliqab, M. Alsharari contributed to formal analysis, writing—review and editing. S. N. Daskalakis, A. Armghan contributed to investigation, resources, writing—review and editing. M. Alsharari, A. Armghan contributed to supervision and project administration. M. Alsharari, K. Aliqab and S. N. Daskalakis contributed to visualization, software, and validation.

Data Availability No datasets were generated or analyzed during the current study.

Declarations

Conflict of interest The authors declare no competing interests.

References

1. Shalaev, V.M.: Optical negative-index metamaterials. Nat. Photonics **1**, 41–48 (2007)
2. Pendry, J.B.: Negative refraction makes a perfect lens. Phys. Rev. Lett. **85**, 3966 (2000)
3. Han, T., Bai, X., Thong, J.T.L., Li, B., Qiu, C.-W.: Full control and manipulation of heat signatures: cloaking, camouflage and thermal metamaterials. Adv. Mater. **26**, 1731–1734 (2014)
4. Ji, Y., Tang, C., Xie, N., Chen, J., Gu, P., Peng, C., Liu, B.: High performance metamaterial sensors based on strong coupling between surface plasmon polaritons and magnetic plasmon resonances. Results Phys. **14**, 102397 (2014)
5. Alam, J., Faruque, M.R.I., Islam, M.T.: Labyrinth double split open loop resonator based bandpass filter design for S, C and X-band application. J. Phys. D Appl. Phys. (2018). https://doi.org/10.1088/1361-6463/aac569
6. Ziolkowski, R.W., Engheta, N.: Metamaterials: two decades past and into their electromagnetics future and beyond. IEEE Trans. Antennas Propag. **68**, 1232–1237 (2020)
7. Rhee, J.Y., Kim, Y.J., Yi, C., Hwang, J.S., Lee, Y.P.: Recent progress in perfect absorbers by utilizing metamaterials. J. Electromagn. Waves Appl. **34**, 1338–1371 (2020)
8. Xu, K., Guo, Y., Liu, Y., Deng, X., Chen, Q., Ma, Z.: 60-GHz compact dual-mode on-chip bandpass filter using GaAs technology. IEEE Electron Device Lett. **42**, 1120–1123 (2021)
9. Chen, H., Chen, W., Liu, X., Liu, X.: Establishing the first hidden-charm pentaquark with strangeness. Eur. Phys. J. **81**, 409 (2021)
10. Liang, S., Xu, F., Li, W., Yang, W., Cheng, S., Yang, H., Chen, J., Yi, Z., Jiang, P.: Tunable smart mid infrared thermal control emitter based on phase change material VO_2 thin film. Appl. Therm. Eng. **232**, 121074 (2023)
11. Armghan, A., Alsharari, M., Baqir, M.A., Saqlain, M., Aliqab, K.: A high-performance ultra-wideband metasurface absorber and thermal emitter for solar energy harvesting and thermal applications. Phys. Chem. Chem. Phys. **26**, 25469–25479 (2024)
12. Pu, M., Hu, C., Wang, M., Huang, C., Zhao, Z., Wang, C., Feng, Q., Luo, X.: Design principles for infrared wide-angle perfect absorber based on plasmonic structure. Opt. Express **19**(18), 17413–17420 (2011)
13. Khichar, V., Hozhabri, N., Koymen, A.R.: Solar energy harvesting using new broadband metamaterial solar absorbers for generation of heat. APL Energy **2**(1), 016105 (2024)
14. Yang, C., Cui, X., Zhang, Z., Chiang, S.W., Lin, W., Duan, H., Li, J., Kang, F., Wong, C.-P.: Fractal dendrite-based electrically conductive composites for laser-scribed flexible circuits. Nat. Commun. **6**(1), 8150 (2015)
15. Pu, M., Feng, Q., Wang, M., Hu, C., Huang, C., Ma, X., Zhao, Z., Wang, C., Luo, X.: Ultrathin broadband nearly perfect absorber with symmetrical coherent illumination. Opt. Express **20**(3), 2246–2254 (2012)
16. Ali, A.M., Ghanim, A.M., Othman, M., Swillam, M.A.: All silicon MIR super absorber using fractal metasurfaces. Sci. Rep. **13**(1), 15545 (2023)
17. Kazerooni, H., Khavasi, A.: Plasmonic fractals: ultrabroadband light trapping in thin film solar cells by a Sierpinski nanocarpet. Opt. Quantum Electron. **46**(6), 751–757 (2014)
18. Yuan, Y., Liu, H., Liu, M., Zhang, W., Li, X., Cheng, S.: Design of wide-angle broadband titanium-nitride solar absorber based on column-cavity structure. Phys. Lett. A (2025). https://doi.org/10.1016/j.physleta.2025.130832
19. Sayed, S.I., Mahmoud, K.R., Mubarak, R.I.: Strong and broadband visible absorption based on titanium patterned resonator. Plasmonics **3**, 1145–1152 (2023)
20. Saqlain, M., Baqir, M.A., Choudhury, P.K.: MXene- and graphene-assisted THz metamaterial for cancer cells detection based on refractive index sensing. IEEE Trans. Nanotechnol. **23**, 652–657 (2024)
21. Shangguan, Q., Zhao, Y., Song, Z., Wang, J., Yang, H., Chen, J., Liu, C., Cheng, S., Yang, W., Yi, Z.: High sensitivity active adjustable graphene absorber for refractive index sensing applications. Diamond Relat. Mater. **128**, 109273 (2022)
22. Houran, M.A., Armghan, A., Baqir, M.A., Aliqab, K., Saqlain, M., Alsharari, M.: MXene nanorods-based metasurface wideband absorber for infrared regime. Int. J. Therm. Sci. **193**, 108452 (2023)
23. Houran, M.A., Abdulrazak, L.F., Baqir, M.A., Saqlain, M., Hassan, A.: Lithography-free polarization-insensitive and wide-angle solar absorber operating in wide spectrum. Int. J. Therm. Sci. **196**, 108713 (2024)
24. Ai, Z., Yi, Y., Yang, H., Liu, M., Yi, Y., Tang, C., Gao, F.: TiN-Ti ultra-broadband solar absorber: efficient heat absorption and high thermal stability. Phys. Lett. A **556**, 130827 (2025)
25. Liu, H., Li, J., Yang, H., Wang, J., Li, B., Zhang, H., Yi, Y.: TiN-only metasurface absorber for solar energy harvesting. Photonics **12**(5), 443 (2025)
26. Yao, X., Yi, Z., Liu, C., Zhang, J., Cheng, S., Zeng, Q., Chen, J., Yi, Y., Tang, C.: Thermal emitter performance of ultra-broadband solar metamaterial absorber based on metal–insulator–metal device structure. Opt. Commun. **570**, 130937 (2024)
27. Lee, D., Han, S.Y., Jeong, Y., Nguyen, D.M., Yoon, G., Muu, J., Chae, J., Lee, J.H., Ok, J.G., Jung, G.Y., et al.: Polarization-sensitive tunable absorber in visible and near-infrared regimes. Sci. Rep. **8**, 12393 (2018)
28. Ding, F., Mo, L., Zhu, J., He, S.: Lithography-free, broadband, omnidirectional, and polarization-insensitive thin optical absorber. Appl. Phys. Lett. **106**(6), 061108 (2015)
29. Haque, A., et al.: Damage analysis of a perfect broadband absorber by a femtosecond laser. Sci. Rep. **9**, 15880 (2029)
30. Chen, L., Sun, L., Dong, H., Mou, N., Zhang, Y.: Near-field imaging of the multi-resonant mode induced broadband tunable metamaterial absorber. RSC Adv. **10**, 5146–5151 (2020)
31. Zou, L., Zou, Y., Wu, B., Liu, H., Li, X., Wu, X.: Ultra-broadband and wide-angle solar absorber with hierarchical nanohole design based on MXene. Int. J. Therm. Sci. **197**, 108764 (2024)

32. Yuan, H., Zeng, Q., Wang, Z., Sun, T., Song, Q., Yi, Z., Liu, Z., Cheng, S., Wu, P.: Ultra-broadband solar absorber and near-perfect thermal emitter based on columnar titanium micro-structure. Appl. Therm. Eng. **262**, 125294 (2025)
33. Qin, F., Chen, X., Yi, Z., Yao, W., Yang, H., Tang, Y., Yi, Y., Li, H., Yi, Y.: Ultra-broadband and wide-angle perfect solar absorber based on TiN nanodisk and Ti thin film structure. Sol. Energy Mater. Sol. Cells **211**, 110535 (2020)
34. Fite, G.M., Maremi, F.T., Gemta, A.B., Hurisa, T.F., Aredo, T.B.: Optimizing light absorption and emission in thermophotovoltaics: a study of tungsten–hafnium dioxide metamaterials. J. Appl. Phys. **137**(8), 083102 (2025)
35. Zhang, Y., Chen, Y., Wang, T., Zhu, Q., Gu, M.: Ultrahigh performance passive radiative cooling by hybrid polar dielectric metasurface thermal emitters. Opto-Electron. Adv. **7**(4), 230194–230201 (2024)
36. Wang, S., Wu, Y., Pu, M., Xu, M., Zhang, R., Yu, T., Li, X., et al.: A versatile strategy for concurrent passive daytime radiative cooling and sustainable energy harvesting. Small **20**(6), 2305706 (2024)
37. Rahman, M.T., Mireles, K., Chavez, J.J.G., Wo, P.C., Marcial, J., Kessler, M.R., McCloy, J., Ramana, C.V., Panat, R.: High temperature physical and chemical stability and oxidation reaction kinetics of Ni–Cr nanoparticles. J. Phys. Chem. C **121**(7), 4018–4028 (2017)
38. Jen, S.-U., Sun, H., Chiang, H.-P., Chen, S.-C., Chen, J.-Y., Wang, X.: Optoelectronic properties and the electrical stability of Ga-doped ZnO thin films prepared via radio frequency sputtering. Materials **9**(12), 987 (2016)
39. Zhang, Y., Evans, J.R.G., Yang, S.: Corrected values for boiling points and enthalpies of vaporization of elements in handbooks. J. Chem. Eng. Data **56**(2), 328–337 (2011)
40. Haynes, W.M.: CRC Handbook of Chemistry and Physics. CRC Press, Boca Raton (2016)
41. Yuan, H., Zeng, Q., Wang, Z., Sun, T., Song, Q., Yi, Z., Liu, Z., Cheng, S., Wu, P.: Ultra-broadband solar absorber and near-perfect thermal emitter based on columnar titanium micro-structure. Appl. Therm. Eng. **262**, 125294 (2025)
42. Wang, J., Zhang, S., Sun, X., Wang, C., Tang, Z., Yu, F., Zhao, Z., Mao, J., Zhang, Q., Cao, F.: Efficient selective planar emitters for thermophotovoltaic systems at 1473 K. Appl. Therm. Eng. (2025). https://doi.org/10.1016/j.applthermaleng.2025.126999
43. Ngobeh, J.M., Sorathiya, V., Alwabli, A., et al.: MXene-based multilayered and ultrawideband absorber for solar cell and photovoltaic applications. Sci. Rep. **15**, 1972 (2025)